JET MIXING OF CRYOGEN AND WATER

Jan Dahlsveen* **Reidar Kristoffersen†** **Lars R. Sætran‡**
Department of Mechanics, Thermo- and Fluid Dynamics
Norwegian University of Science and Technology, N-7491 Trondheim, Norway

ABSTRACT

This paper contains description of experiments with liquefied nitrogen jets injecting into water, where the jet penetration depth below the water surface is measured. The results are compared with numerical simulations by a axis-symmetric premixing code. Experiments and simulations show that the penetration depth is dependant on the jet buoyancy and momentum flux, but that there is little mixing of cryogen with water. Comparisons are made with experiments with small scale and industrial scale releases, and good agreement with penetration depth and plume geometry is found.

INTRODUCTION

When LNG is spilled onto water the heat transfer from water to LNG may be so fast that a Rapid Phase Transition (RPT) of the LNG may occur. The severity of the RPT is dependant on the amount of cryogen that is mixed with water, and this premixed volume is characterized by a *penetration depth* and a *width/spreading angle* (Gabillard et al., 1996). Small scale experiments are performed along with numerical simulations with a premixing code (Dahlsveen, 1999), originally written for melt/water mixing. Most of the earlier studies of coarse mixing have been performed in the metal and nuclear industries, including works by e.g. Epstein and Fauske (1985), Corradini (1988), Wang et al. (1989) and Fletcher and Thyagaraja (1991).

A cryogen jet spill over water may be divided into three zones, see Figure 1:

- The zone close to the nozzle, where the jet injects into air. The jet spreads out and eventually breaks up into separate drops.
- The zone below the water surface where the cryogen mixes with water.
- The rising plume outside the mixing zone.

The last two regions are characterized by violent turbulent mixing and evaporation.

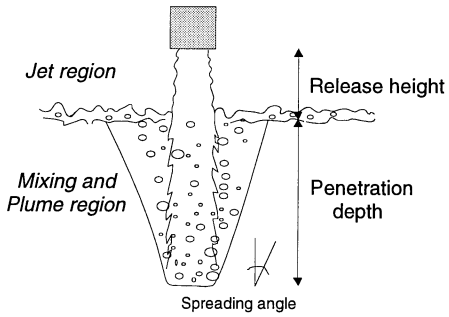

Figure 1: Cryogen spill over water, with different regions and characteristic parameters.

PREMIXING REGION

A jet injected into water is buoyant if the jet fluid is of a different density than that of the surroundings. The ratio between the momentum and buoyancy forces of the jet can be expressed as the Richardson-number:

$$Ri = \frac{gR\Delta\rho}{U^2\rho} \tag{1}$$

where $\Delta\rho$ is the difference between densities of evaporated jet fluid and water, and R is the radius of the jet.

Assuming that the liquefied nitrogen evaporates quickly, the equivalent momentum and bouyancy flux of the jet, based on the density of the gas after evaporation, can be determined. This kind of negative buoyant and reversing buoyancy flows have been studied by many researchers, e.g. Goldman (1986), Turner (1966) and Cresswell (1993).

A dimensionless mean jet penetration depth scaled with jet radius can be expressed in terms of the Richardson number Ri:

$$\frac{Z_m}{R} = CRi^b \tag{2}$$

where $b = -\frac{1}{2}$ from dimensional analysis. The constants C and b cited in the litterature

*Jan.Dahlsveen@mtf.ntnu.no
†Reidar.Kristoffersen@mtf.ntnu.no
‡Lars.Satran@mtf.ntnu.no

varies, but $C \sim 4$ and $b = -0.5$ makes the closest fit with Turners results.

1-D APPROACH

The sketch in Figure 1 shows a buoyant jet injected vertically into water. The oscillating (or pulsating) motion observed is a result of time varying forces from buoyancy and momentum acting on the jet coloumn. Simplifying and assuming the motion to be one-dimensional the dynamics of the jet coloumn may be modelled through Newtons 2nd law:

$$\rho_c \pi R^2 z \frac{d^2 z}{dt^2} = \rho_c \pi R^2 \frac{1}{2} U_0^2 - \pi R^2 z \Delta \rho g \quad (3)$$

Linearizing the acceleration term, $z\ddot{z} \approx L\ddot{z}$, the equation has a sinusiodal analytical solution with frequency, $\omega_0 = \frac{g}{U_0}\sqrt{2\frac{\Delta\rho}{\rho_c}}$, centered around an average penetration depth, $z_m = \frac{\rho_c}{\Delta\rho}\frac{U^2}{2g}$.

PREMIXING MODELLING

The present axis-symmetric premixing code is transient and models the hydrodynamics of three species: cryogen, its vapour and water, solving the multiphase flow equations for the conservation of mass, momentum and energy. The following assumptions are made:

- The cryogen liquid and vapor are assumed to be at the saturation temperature
- Incompressible flows
- The cryogen liquid is composed of spherical droplets

The multiphase flow equations are solved using a finite difference method using staggered grids. All the convection terms are upwind discretized for stability.

The premixing model is validated through small scale experiments and experiments performed on a large scale (Gabillard et al., 1996).

Governing equations

The volume fractions for the different species water (w), cryogen (c) and its vapor (v) gives the relation

$$\alpha_w + \alpha_c + \alpha_v = 1 \quad (4)$$

Using cylindrical coordinates r and z with corresponding velocity components U and V, the mass conservation of species i take the form

$$\frac{\partial}{\partial t}(\alpha_i) + \frac{1}{r}\frac{\partial}{\partial r}(r\alpha_i U_i) + \frac{\partial}{\partial z}(\alpha_i V_i) = \frac{\dot{m}_i}{\rho_i} \quad (5)$$

where $\dot{m}_i$ is the mass exchange rate. Since water is assumed not to evaporate, $\dot{m}_w = 0$ and so $\dot{m}_c + \dot{m}_v = 0$. The momentum equations in the radial and axial directions yield

$$\frac{\partial}{\partial t}(\alpha_i \rho_i U_i) + \frac{1}{r}\frac{\partial}{\partial r}(r\alpha_i \rho_i U_i^2) + \frac{\partial}{\partial z}(\alpha_i \rho_i U_i V_i) = \alpha_i \frac{\partial p}{\partial r} + F_{Di}^r + F_{mi}^r \quad (6)$$

and

$$\frac{\partial}{\partial t}(\alpha_i \rho_i V_i) + \frac{1}{r}\frac{\partial}{\partial r}(r\alpha_i \rho_i U_i V_i) + \frac{\partial}{\partial z}(\alpha_i \rho_i V_i^2) = \alpha_i \frac{\partial p}{\partial z} + F_{Di}^z + F_{mi}^z \alpha_i \rho_i g \quad (7)$$

Assuming that the cryogen conserves the momentum when evaporating, the momentum exchange due to component change becomes $\overrightarrow{F_{mv}} = \dot{m}_v \overrightarrow{v_c}$ and $\overrightarrow{F_{mc}} = -\overrightarrow{F_{mv}}$ The momentum exchange due to interfacial drag is given by

$$\overrightarrow{F_{Dw}} = K_{wc}(\overrightarrow{v_c} - \overrightarrow{v_w}) + K_{wv}(\overrightarrow{v_v} - \overrightarrow{v_w})$$

$$\overrightarrow{F_{Dc}} = K_{wc}(\overrightarrow{v_w} - \overrightarrow{v_c}) + K_{vc}(\overrightarrow{v_v} - \overrightarrow{v_c})$$

$$\overrightarrow{F_{Dv}} = K_{wv}(\overrightarrow{v_w} - \overrightarrow{v_v}) + K_{vc}(\overrightarrow{v_c} - \overrightarrow{v_v})$$

The drag factor for species i caused by species j are

$$K_{ij} = \frac{3}{4}\frac{C_D}{L_i}\rho_a \alpha_i \alpha_j |\overrightarrow{v_j} - \overrightarrow{v_i}| \quad (8)$$

derived by analogy with the drag force on a single droplet of lengthscale L_i falling in a surrounding fluid (species j and k) of density

$$\rho_a = \frac{\rho_j \alpha_j + \rho_k \alpha_k}{\alpha_j + \alpha_k} \quad (9)$$

The lengthscale of the vapor is kept constant, while the lengthscale of water and cryogen is modelled by a transport equation

$$\frac{\partial}{\partial t}(\alpha_i \rho_i L_i) + \frac{1}{r}\frac{\partial}{\partial r}(r\alpha_i \rho_i U_i L_i) + \frac{\partial}{\partial z}(\alpha_i \rho_i V_i L_i) = \dot{L}_i + \dot{m}_i L_i \quad (10)$$

The rate of change of the lengthscale of component i is given by

$$\dot{L}_i = -C_0 \alpha_i |\overrightarrow{v_a} - \overrightarrow{v_i}| \sqrt{\rho_a \rho_i} \quad (11)$$

where C_0 is an empirical constant (~ 1) and $\overrightarrow{v_a}$ is the velocity of the surrounding fluid (species j and k) defined as

$$\overrightarrow{v_a} = \frac{\overrightarrow{v_j}\rho_j \alpha_j + \overrightarrow{v_k}\rho_k \alpha_k}{\alpha_j + \alpha_k} \quad (12)$$

The cryogen is assumed to exist as a dispersed phase of drops, requiering that the length-scale of the jet is specified initially. In the code the initial length scale of the drops is computed by the jet Weber-number. The conservation of energy for water is simplified by assuming that the total enthalpy is the same as its internal energy e, and only account for the rate of heat transfer from the cryogen to water $\dot{q}_{cw}$:

$$\frac{\partial}{\partial t}(\alpha_w \rho_w e_w) + \frac{1}{r}\frac{\partial}{\partial r}(r\alpha_w \rho_w U_w e_w) + \frac{\partial}{\partial z}(\alpha_w \rho_w V_w e_w) = \dot{Q}_{cw} = \dot{m}_v h_{fg} \quad (13)$$

where h_{fg} is the latent heat of vaporization of the cryogen liquid. Following Fletcher and Thyagaraja, the rate of vapor production is given by

$$\dot{m}_v = 6\alpha_w \alpha_c h(T_w - T_{sat})/(L_c h_{fg}) \quad (14)$$

where T_{sat} is the saturation temperature. The heat transfer coefficient h is determined by taking the maximum of the forced convection and free convection film boiling coefficients for a sphere of diameter L_c.

Solution algorithm

The equations are discretisized on a staggered grid using finite differences. The convective terms are upwind differenced for stability. The solution is marched forward in time by:

1. Determine α_w by solving the continuity equation for water using an explicit scheme,
2. Solve the equation for L_w and $\dot{q}_w$ explicitly,
3. Determine e_w and T_w,
4. Solve equation for $\dot{m}_v$,
5. Determine α_c (and hence α_v) by solving the continuity equation for cryogen using the new vales of all quantities except L_c,
6. Solve equation for L_c,
7. Calculate the tentative velocity fields based on the available pressure field,
8. Evaluate pressure correction coefficients using the continuity equation with the tentative velocity field and the new volume fractions,
9. If the local continuity error is too large, update pressure and velocity fields using a conjugate gradient solver, and go to step 7.

Drag-coefficient C_D

The drag-coefficient of spherical particles is $C_D = 0.4$ (White, 1986). When using this value for C_D, the jet continues to penetrate deeper below water than found in the experiments. In a paper presented by Fletcher (1988), where validation experiments with steel spheres falling in water were presented, it was shown that increasing the drag-coefficient in his premixing code made it possible to simulate the metal-jet more closely. In the present simulations the drag-coefficient $C_D = 2.5$.

SMALL-SCALE EXPERIMENTAL SETUP

The liquefied nitrogen jet is ejected from a nozzle into a 2500 mm diameter water tank with a maximum water depth of 800 mm. By pressurizing the liquefied nitrogen gas tank, the nitrogen flows through a pipe-system to a pneumatically controlled nozzle, measuring the volume-flow by a volume-flow-meter. A

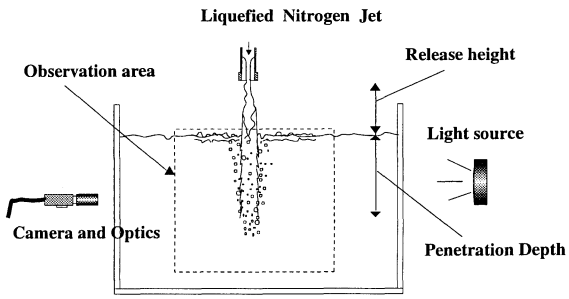

Figure 2: Experimental setup and instrumentation for visualizing the jet experiments.

'shadow-graph' visualization technique is used to study the mean penetration depth of the jet. The images are captured by a CCD-camera, and processed by an image-processing program. A 500 W incandescent lamp is placed at the opposite side of the water tank from the camera, as shown in Figure 2.

LARGE SCALE EXPERIMENTAL SETUP

The large scale experiments were conducted the same way as the small scale experiments, injecting cryogen from a 50 and 100 mm nozzle from 1 meter above the water surface into a 40 meter diameter pond. The jet velocities

ranged from 3 – 18 m/s. The penetration depth was monitored by video-filming, measuring the jet mean penetration depth and jet pulsation frequency.

RESULTS

The following was observed during the liquefied nitrogen jet releases on both the small and the large scale:

- The initial jet stem penetrates the water surface and goes straight down; evaporation at the sides of the jet starts
- The jet stem evaporates and the plume diameter increases
- The plume rises, and a new stem penetrates through the plume and starts to evaporate
- The jet/water mixing continues with a pulsating behavior with some deviation around the mean penetration depth.

Figure 3 shows a picture with an average of 32 still-images grabbed in the steady-state release period, lasting typically for 7 to 14 seconds. Each grabbed image is processed and converted to a binary picture (black/white) before they are averaged and give a picture with 32 grey tones. The mean penetration depth and mean plume spreading angle can be measured.

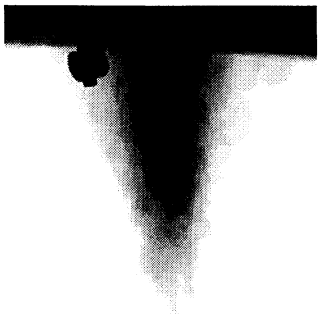

Figure 3: Gray-scale image with 32 averaged still images taken in the 'steady-state' period of the release.

In Figure 4 the dimensionless penetration depth from the present small scale experiments, Turners experiments and the large scale jet experiments are plotted against the jet Richardson number (ratio of buoyancy to momentum force). A wide range of Richardson numbers are covered in these experiments ($Ri = 0.001 - 0.07$).

The results from the present small scale jet experiments fit well with the results by Turner given by the Equation 2, with the constants $b = -1/2$ and $C = 4.0$, with the smallest jet diameter (8 mm) giving the closest fit. The 16 mm diameter jet and the large scale jet experiments are best correlated with $C = 5.8$. It is shown that the nitrogen jet experiments in the range $8 - 100$ mm follows the same relation for penetration depth, based on jet Richardson number.

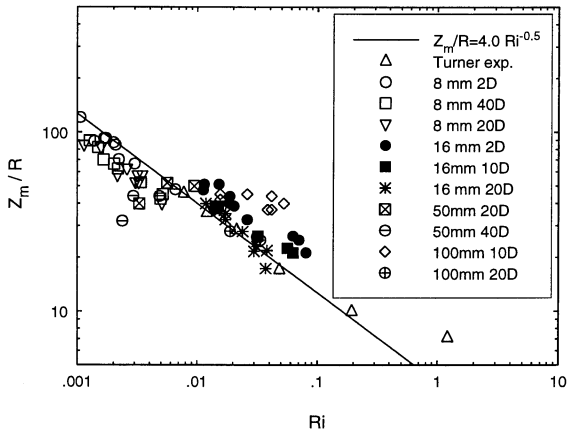

Figure 4: Penetration depth measurements compared with Turners results and correlation and large scale liquefied nitrogen jet experiments.

Simulations

In Figure 5 the simulated penetration depth history for an industrial scale spill is shown. The nozzle diameter is 100 mm and the volume flow is 45 liters/s, making the jet velocity 5.7 m/s; release height above the water surface is 1 meter. The simulated mean penetration depth is approximately 2.3 meters in the steady state period of the spill, close to the result reported in the experiments (2.2 meters). The penetration depth varies with a characteristic time of approximately 3 seconds, similar to the time scale reported by in the large scale tests. The case is simulated with 75 times 75 grid cells.

The velocity of the small scale jet is 2.6 m/s, with mean penetration depth higher in the simulations (0.7 m) than in the experiments (0.41 m), but with similar characteristic penetration frequency. In Table 1 the mean penetration depth and frequency for the 1D approach, experiments and simulations are presented.

In Figure 6 the volume fraction of vapor for the axis-symmetric simulation is shown. The symmetry axis is at the left side of the figure. The plume consists of a stem of liquefied cryogen (dark gray), surrounded by a relatively thin layer og vapor (light gray). The surrounding water is black.

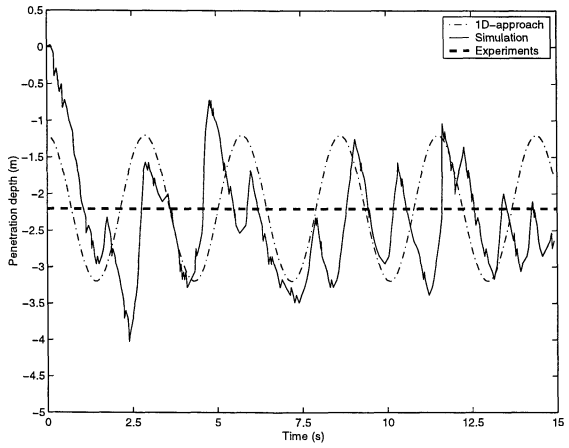

Figure 5: Penetration depth history, $Z_m(t)$ of large scale jet release, $Q = 45$ liters/s, $D = 100$ mm and $U = 5.7$ m/s.

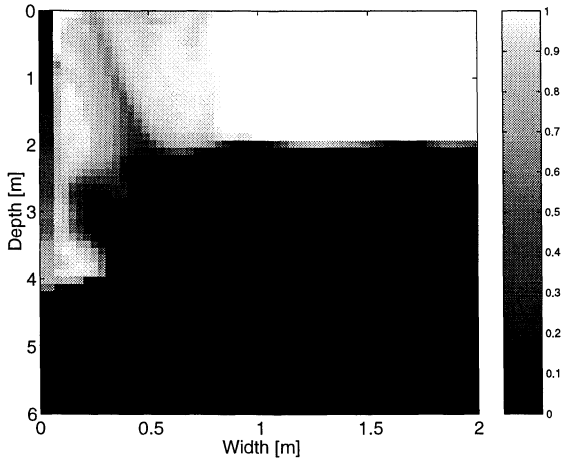

Figure 6: Volume fraction of gas, α_2, from simulation. $Q = 45$ liters/s, $D = 100$ mm and $U = 5.7$ m/s. Time, $t = 10$ seconds.

$U_0[m/s]$	$Z_m[m](meas./sim.)$	$Period[s](meas./sim./1D)$
2.6	0.41 / 0.7	0.8 / 1.0 / 1.2
5.73	2.2 / 2.3	3.0 / 2.8 / 3.2

Table 1: Comparisons between experiments and simulations.

Plume spreading angle

The spreading angle for the rising plume, β, after vaporization is measured from the captured and processed grey-scale images. The mean spreading-angle is defined as the angle between the center line and the line drawn along a countour where the image intensity is 128. This corresponds to the 'half' width of the concentration, i.e half-width of plume spreading based on mean void fraction in the plume.

The mean spreading-angles in the 16 mm and 100 mm jet-experiments were $\beta = 12 - 15°$ and $\beta = 14 - 22°$, respectively, width increasing angle for increasing volume flow. The results show that the nitrogen-jet, when evaporated, rises similarly to a gas plume in water, but the mean spreading angle is larger than for a buoyant plume, which has a typical spreading angle of ~ 7 degrees (Fischer, 1979). The reason for a wider spread of a cryogen plume may be due to the effect of the downward moving jet stem in the middle of the plume forcing the plume outwards.

In a three seconds period from the jet simulation, 32 snapshots of the gas fraction were taken, and the average is shown in Figure 7. The mean plume spreading angle is ~ 14 degrees.

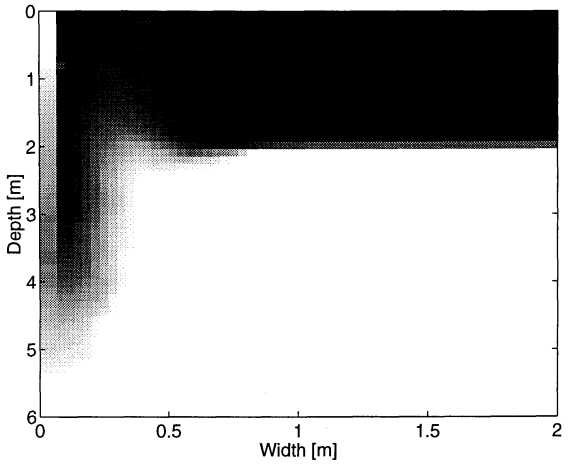

Figure 7: Averaged image of gas fraction, α_2 from simulation. $Q = 45$ liters/s, $D = 100$ mm and $U = 5.7$ m/s. Time, $t = 2 - 6$ seconds.

CONCLUSIONS

- The mean penetration depth below the water-surface showed direct dependency with the jet Richardson number for both small (16 mm) and large jet diameters (100 mm). Simulations on small and large scale give similar results.
- The characteristic penetration frequencies for the experiments and simulations are similar, with highest frequencies for smallest volume-flows
- Very little mixing between water and liquefied nitrogen occurs before the nitrogen evaporates. This indicates that most of the heat-transfer from the water to the nitrogen jet occurs while it is 'un-broken', i.e. while the jet is like a continous stem surrounded by a blanket of vapor.
- The present relation between the penetration depth and jet Richardson number of the spill can give an estimate of the maximum volume of cryogen that can take part in an RPT.

REFERENCES

Corradini, M.L. Kim, B.J., Oh, M.D., 1988, "Vapor explosions in light water reactors: A review of theory and modeling". *Progr. in Nuc. Energy.* Vol. 22, No. 1, pp. 1-117.

Cresswell, R.W., Szczepura, R.T., 1993, "Experimental investigation into a turbulent jet with negative buoyancy". *Phys. Fluids.* A 5 (11), Nov.

Dahlsveen, J., 1999, "Rapid Phase Transitions - A study of mixing and fragmentation". Ph.D. Thesis. Norwegian University of Technology and Science, Trondheim, Norway.

Epstein, M., Fauske, H. K., 1985, "Steam film instability and the mixing of core-melt jets and water". *ANS proceedings. National heat transfer conference.* Aug. 4- 7. Denver, Colorado.

Fischer, H.B. et al., 1979, 'Mixing in Inland and Coastal waters'. Chapter 9, p.329-332. ISBN: 0-12-258150-4.

Fletcher, D.F. *The particle distribution of solid melt debris from molten fuel-coolant interaction experiments.* Nucl. Engng. Des., 105, 313-319. 1988.

Fletcher, D.F., Thyagaraja, A., 1991, "The CHYMES mixing model". *Progress in Nucl. Energy.* Vol. 26, No. 1, pp. 31-61.

Gabillard, M., Dahlsveen, J., Cronin, P., 1996, "Rapid Phase Transition of Liquefied Gas". *European Applied Research Conference on Natural Gas - Eurogas-96.* Norwegian University of Science and Technology, Trondheim, Norway.

Goldman, D., Jaluria, Y., 1986, "Effect of opposing buoyancy on the flow in free and wall jets". *J. Fluid. Mech.*, Vol. 166, pp. 41-56.

Turner, J.S., 1966, "Jets and plumes with negative or reversing buoyancy". *J. Fluid Mech.*, vol. 26 part 4, pp. 779-792.

Wang, S.K., Blomquist, C.A., Spencer, B.W., 1989, "Modelling of thermal and hydrodynamic aspects of molten jet/water interactions". *ANS Proceedings - National Heat Transfer Conference*, Aug., Philadelphia, Penn.

White, F.M., 1986, *Fluid Mechanics.* McGraw-Hill. 2nd edition.